II. MICROWAVE SPECTROSCOPY*

Prof. M. W. P. Strandberg
Prof. R. L. Kyhl
Dr. J. M. Andrews, Jr.
A. Fukumoto
J. G. Ingersoll
J. D. Kierstead
M. K. Maul
T. E. McEnally
S. Reznek
L. Rozen
W. J. Schwabe

A. WORK COMPLETED

1. A STUDY OF SUPERCONDUCTING DOMAIN STRUCTURES USING OPTICAL POLARIZATION TECHNIQUES

This work has been completed by Lowell Rosen and submitted as a thesis to the Department of Physics, M. I. T., August 1965, in partial fulfillment of the requirements for the degree of Master of Science. An abstract of the thesis follows.

The superconducting magnetic structures of Tantalum have been studied by using the effect of optical Faraday rotation in Cerous Metaphosphate glass. Photographs of the Tantalum specimen showing both the intermediate and mixed states of the metal are included. The sequence of magnetization pictures shows the magnetic structures as the magnetic field is first increased in one direction, decreased to zero, and then increased in the opposite direction. Part of the sequence of photographs clearly indicates the phenomenon of the flux-jumping characteristic of Type II and hard superconductors.

M. W. P. Strandberg

2. THE LOW-TEMPERATURE USE OF ELECTROLYTIC CAPACITORS AND BIFILAR PULSE TRANSFORMERS

A Master's thesis with this title has been submitted by Michael K. Maul to the Department of Electrical Engineering, M. I. T., August 1965. A summary of the thesis follows.

The use of electrolytic capacitors and bifilar pulse transformers in liquid Helium has been found to be practical if the following conditions are noted. The capacitance at 4.2°K of Sprague 150° tantalums is 15 per cent of the room-temperature value. The values measured were in the range 1 mfd-47 mfd at room temperature.

Bifilar transformers with ferrite cores were found inadequate to pass 1 μsec pulses at 4.2°K. This was due to the large decrease in permeability as the temperature decreases. YIG was found to have a sufficiently low loss of permeability to pass these pulses.

R. L. Kyhl

*This work was supported principally by the Joint Services Electronics Program (Contract DA36-039-AMC-03200(E).

(II. MICROWAVE SPECTROSCOPY)

B. INCOHERENT PHONON PROPAGATION IN X-CUT QUARTZ

There is some evidence to indicate that the unknown signals reported in previous experiments[1,2] are caused by ringing in the pulse circuit. At low temperatures the source impedance of our superconducting bolometer usually was decreased to values that were of the order of 0.1 Ω, a value that is somewhat lower than the series resistance in the stainless-steel transmission line and numerous coaxial adapters that were used for the video signal. These conditions can produce ringing in a pulse transformer circuit. In a series of subsequent experiments we increased the impedance of the bolometric film by removing portions of it after the leads were attached. This is shown in

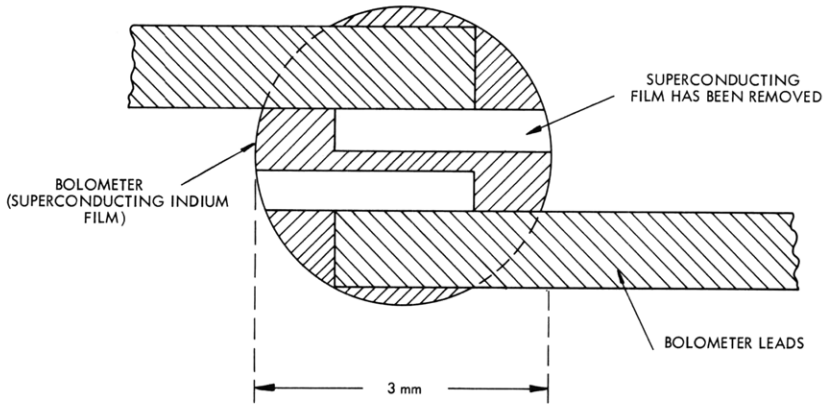

Fig. II-1. Bolometer geometry. Illustrating schematically the manner in which the low-temperature impedance of the superconducting bolometer was increased from 0.1 to 1 Ω by removing portions of the film.

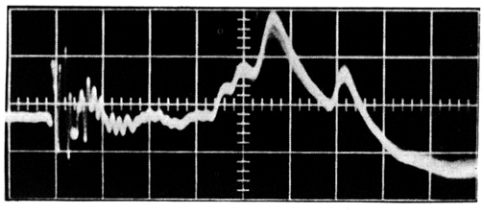

Fig. II-2.

Pulses of incoherent phonons in x-cut quartz. Four distinct pulses are resolved by the 1-Ω bolometer. All have been accounted for theoretically. The L stands for longitudinal; FT, fast-transverse; ST, slow-transverse; O, oblique. Oscilloscope sweep rate, 1 μsec/cm.

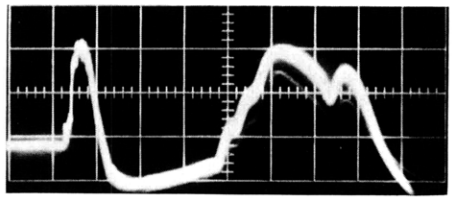

Fig. II-3.

Pulses of incoherent phonons in x-cut quartz at a power level close to breakdown in the waveguide. Elastic dispersion in the quartz is beginning to produce an observable effect on the pulsewidth. A shift in the peak of the pulse in the direction of increasing time was also observed.

detail in Fig. II-1. Signals detected by this bolometer did not reveal any more than four distinct pulses: the three pure modes and the oblique mode discussed at length in the previous report.[2] In Fig. II-2 we show a typical incoherent phonon signal in an x-cut quartz rod 19 mm long detected by the 1-Ω bolometer. The sweep rate is 1 μsec/cm.

We increased the microwave power incident upon the aluminum film that generates the heat pulse in an attempt to display the dispersion effects that we expect from the theoretical discussion of the preceeding section. At a power level extremely close to the onset of breakdown in the waveguide we were able to obtain the trace shown in Fig. II-3. Because of an intermittent breakdown problem in the waveguide, we could only estimate that the incident peak power was several kilowatts. Pulse broadening is quite evident, and a shift of the peak of the pulse in the direction of increasing time was observed. A detailed comparison of these pulse shapes with the theory presented in Sec. II-C will require a video amplifier with an increased bandwidth.

The author wishes to express his appreciation to Mr. M. C. Graham who carried out the experiments.

J. M. Andrews, Jr.

References

1. J. M. Andrews, Jr., "Observations of Incoherent Phonon Propagation in X-cut Quartz," Quarterly Progress Report No. 77, Research Laboratory of Electronics, M.I.T., April 15, 1965, pp. 7-15.

2. J. M. Andrews, Jr., "Incoherent Phonon Propagation in X-cut Quartz," Quarterly Progress Report No. 78, Research Laboratory of Electronics, M.I.T., July 15, 1965, pp. 10-15.

C. INCOHERENT PHONON PROPAGATION IN A BORN-KÁRMÁN LATTICE

The simplest model that includes dispersion in a description of the lattice dynamics of a three-dimensional crystal is that proposed originally by Born and von Kármán.[1] This model treats a crystal as an elastically isotropic continuum except that the linear dispersion relationship has been replaced by the sinusoidal dispersion function obtained from the one-dimensional linear chain model. From some of the x-ray studies of lattice vibrations[2] it would appear that a sinusoidal dispersion relation is a reasonably good representation, provided that the phase of the function can be scaled to fit the experimental data.

Phonon dispersion in crystalline quartz has recently been studied by neutron diffraction techniques.[3] There is good agreement between the experimental results obtained along the c crystallographic axis and the theory based upon a Born-Kármán model. We are interested, however, in the dispersion of the acoustic modes whose wave vectors are directed along the x axis. The results of a calculation based upon the Born-Kármán

model are shown in Fig. II-4. The frequencies of the three acoustic branches of the vibrational spectrum have been plotted as a function of the x component of the elastic

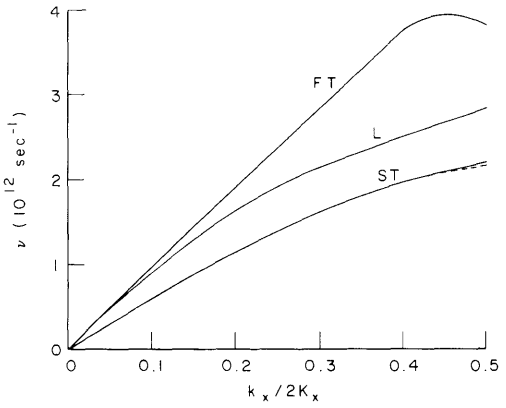

Fig. II-4.

Elastic dispersion in a Born-Kármán lattice. Solid lines were calculated by Elcombe.[4] L stands for longitudinal polarization; FT, fast-transverse; ST, slow-transverse. The dotted line is the sinusoidal function of Eq. 1.

wave vector. These are shown by the solid lines in the figure. We have attempted to approximate the dispersion of the slow-transverse mode by a sinusoidal function given by

$$\nu = \nu_o \sin\left(\frac{\epsilon \pi k_x}{2K_x}\right) \text{sec}^{-1}, \tag{1}$$

where ν is the frequency of the mode, ν_o is the maximum frequency of the mode that can be transmitted along the x axis of the crystal; ϵ is an adjustable parameter of approximately unity, k_x is the x component of the elastic wave vector, and K_x is the edge of the Brillouin zone in the x direction. We have fitted this function to the slow-transverse mode by choosing $\epsilon = 0.88$ and $\nu = 2.21 \times 10^{12}$ sec^{-1}. Equation 1 is shown by the dotted line in Fig. II-4.

We wish to examine the nature of the propagation of an incoherent superposition of fast-transverse elastic modes in α quartz whose wave vectors are all directed along the x crystallographic axis, but whose frequencies are characterized by a black-body distribution function. We seek a function P(t,x) that represents the rate of elastic energy flow at any time t and at any point x along an x-cut rod. We shall assume that the temperature of the quartz is at absolute zero and the crystal is perfect so that the frequency-dependent scattering process can be neglected. In order to represent the quantity P(0, 0) as a Dirac delta function,

$$P(t, 0) = W\delta(t) \text{ watts}. \tag{2}$$

When this function is integrated over all time, we obtain the total energy, W joules, contained in the thermal spike represented by Eq. 2. The spatial character of the function is contained in the expression

$$P(0, x) = UV\delta(x/v) \text{ watts}, \tag{3}$$

where U is the elastic energy density, and V is an arbitrary volume. Since

$$\frac{dW}{dx} = \frac{dW}{dt}\frac{dt}{dx} = \frac{P(0, x)}{v}, \tag{4}$$

the entire energy of the thermal spike at t = 0 can be obtained again by integration of Eq. 4 from $-\infty < x < +\infty$. Since this is equal to the integral of Eq. 2, we have

$$W = UV. \tag{5}$$

The physical interpretation of the volume V can be clarified by noting that a thin metallic film evaporated onto the end of a crystalline quartz rod can be excited by microwave power of extremely short duration, τ. This pulse injects energy into the elastic modes of the crystal, and for those modes whose velocity is v and whose wave vectors are directed along the axis of the rod, this energy is initially contained within a volume

$$V = Av\tau, \tag{6}$$

where A is the cross-section area of the rod. The velocity v of the modes is actually a function of their frequency ν, according to Eq. 1, but in the limit $\nu \to 0$ this has no effect on the normalization volume, V.

The elastic energy density U is assumed to be characterized by a black-body distribution

$$U = \int_0^{\nu_o} \frac{h\nu g(\nu)\, d\nu}{e^{\frac{h\nu}{k_B T}} - 1}, \tag{7}$$

where h is Planck's constant, k_B is Boltzmann's constant, T is the absolute temperature, and $g(\nu)$ is the density of states. The thermal power as a function of time and space P(t, x) of a heat pulse, whose initial form can be characterized by a Dirac delta function, is therefore given by

$$P(t, x) = Av\tau \int \frac{h\nu g(\nu)\, \delta(t-x/v)\, d\nu}{e^{\frac{h\nu}{k_B T}} - 1}, \tag{8}$$

Recall that v is the group velocity of the thermal phonons, and can be obtained by differentiating Eq. 1:

$$v = 2\pi \frac{d\nu}{dk} = \frac{\epsilon \pi^2 \nu_o}{K_x} \cos\left(\frac{\epsilon \pi k_x}{2K_x}\right) \tag{9}$$

or

$$v(\nu) = v_o\left[1-(\nu/\nu_o)^2\right]^{1/2}, \tag{10}$$

where

$$v_o = \frac{\epsilon\pi^2\nu_o}{K_x}.$$

The limiting group velocity for very low frequencies is v_o.

The usual approximation for the elastic density of states in the Born-Kármán lattice is to assume that the modes are distributed equally over a sphere in wave-vector space. This yields

$$g(\nu)\,d\nu = \frac{3k^2}{2\pi^2}\left(\frac{dk}{d\nu}\right)d\nu. \tag{11}$$

If the anisotropy of quartz is neglected, Eqs. 1 and 11 yield

$$g(\nu) = \frac{12\pi\nu_o^2}{v_o^3}\left[\sin^{-1}(\nu/\nu_o)\right]^2\left[1-(\nu/\nu_o)^2\right]^{-1/2}. \tag{12}$$

This density-of-states function has been plotted as a function of the reduced frequency parameter (ν/ν_o) in Fig. II-5. There is a singularity at $\nu/\nu_o = 1$, and the Van Hove

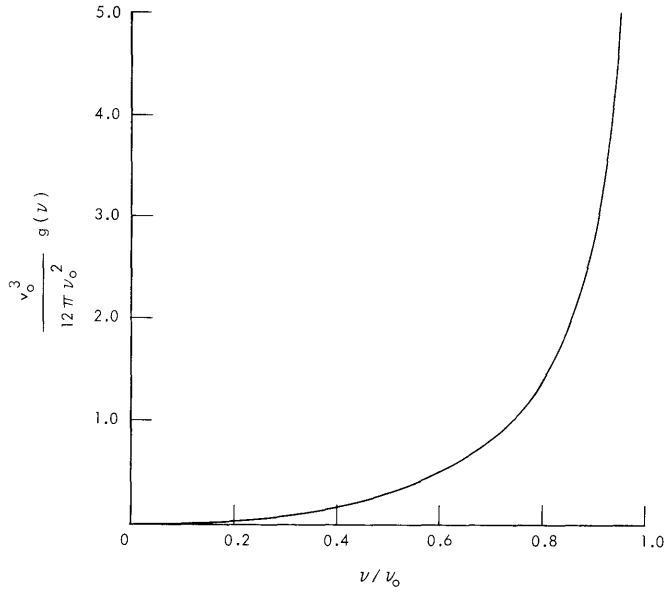

Fig. II-5.

Elastic density of states in a Born-Kármán lattice. This model produces a singularity at ν/ν_o and the Van Hove critical points[5] are absent, but the behavior of $g(\nu)$ at low frequencies is typical of some of the experimentally determined vibration spectra of solids.[2]

critical points[5] do not exist. The low-frequency portion of this function, however, reproduces the experimentally determined vibrational spectra of crystals[2] quite well. At

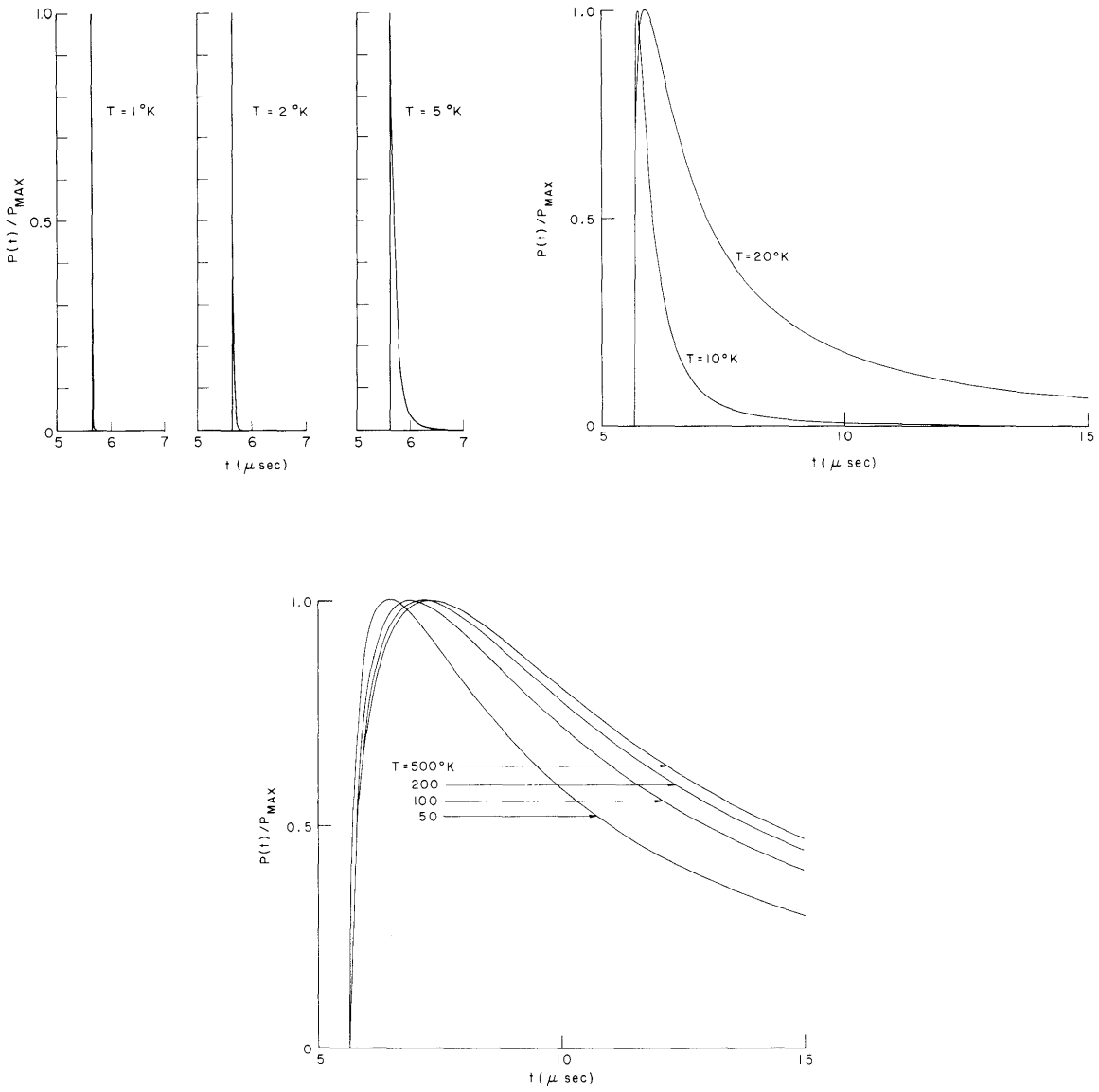

Fig. II-6. Thermal spike that has been propagated through a Born-Kármán lattice. The frequency distribution of the phonons composing the spike has been characterized by black-body distributions at varying temperatures between 1°K and 500°K. The effects of dispersion become very pronounced at the higher temperatures.

temperatures close to absolute zero, Eq. 12 can be used as an excellent approximation.

The elastic density-of-states function $g(\nu)$ given by Eq. 12 is introduced into Eq. 8. The integration variable is changed to

$$t' = v_o \left[1-(\nu/\nu_o)^2\right]^{-1/2}, \tag{13}$$

and we obtain

$$P(t, x) = \frac{12\pi hA\tau\nu_o^4}{xv_o} \begin{cases} (u\cos^{-1} u)^2 \left(e^{\gamma\sqrt{1-u^2}} - 1\right)^{-1} & x/v_o < t < \infty \\ 0 & t \leq x/v_o \end{cases} \tag{14}$$

where

$$u = x/v_o t \qquad \gamma = h\nu_o/k_B T.$$

We have evaluated Eq. 14 for the slow-transverse mode in an x-cut quartz rod, 3 mm in diameter and 19 mm long. The value for v_o is the experimentally determined ultrasonic velocity 3.36×10^5 cm/sec, and the value for ν_o was obtained by fitting a sinusoidal,

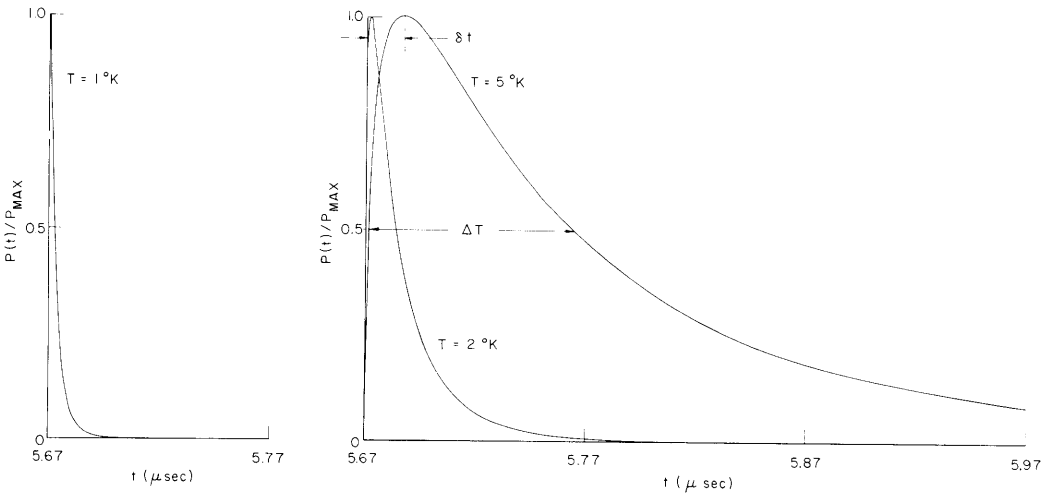

Fig. II-7. Magnified view of Fig. II-6 for T = 1°, 2°, 5°K. This shows the maximum in each curve very close to $t = x/v_o$.

function to the data of Elcombe, as shown in Fig. II-4 ($\nu_o = 2.21\times10^{12}$ sec^{-1}). Equation 14 has been plotted in Fig. II-6 as a function of time t for various values of the absolute temperature T ranging from 1.0 to 500°K. If we recall that at very low temperatures only the lowest elastic modes are excited and that these low-lying modes

exhibit very little dispersion, it is reasonable to expect that the sharp thermal spike initiated into the crystal is very nearly reproduced at x = 19 mm when the temperature that characterizes the black-body distribution is at 1°K. Detail of the first three thermal

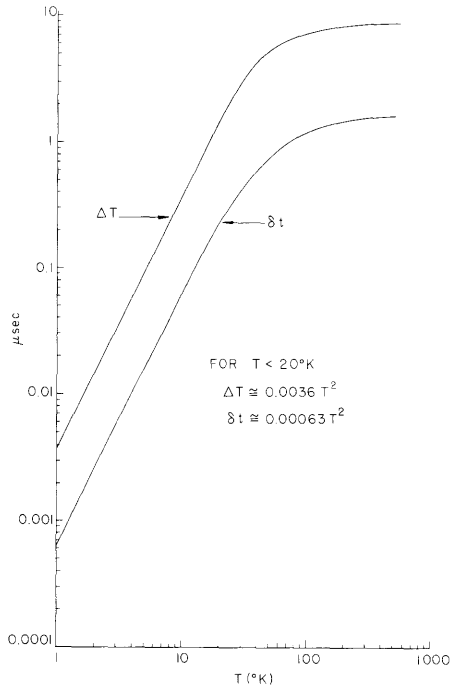

Fig. II-8.

Curve Δt shows variation in the width of the heat pulse at the half-power point ($P/P_{max}=0.5$) as a function of absolute temperature. The shift in the peak of the heat pulse away from $t = x/v_o$ is shown as a function of absolute temperature by δt. Below T = 20°K both curves are very nearly proportional to the square of the absolute temperature.

spikes is shown in Fig. II-7, where the abscissa has been expanded in order to show the maxima more clearly. This occurs very close to $t = x/v_o$ the proper time for an ultrasonic pulse exhibiting no dispersion. Returning to Fig. II-6, we can see that the effect of dispersion becomes very pronounced at higher temperatures as the thermal spike broadens out and its peak moves in the direction of increasing time. In Fig. II-6 the quantity Δt indicates the width of the heat pulse at $P/P_{max} = 0.5$. The shift of the peak of the pulse away from $t = x/v_o$ is indicated by δt. These data are plotted as a function of temperature in Fig. II-8. Up to about 20°K both of these quantities are very nearly proportional to the square of the absolute temperature. Elastic dispersion effects are most evident in the magnitude of the width Δt, which is approximately six times the shift δt in the peak.

J. M. Andrews, Jr.

References

1. M. Born and T. von Karman, Physik. Z. 13, 297 (1912); 14, 15 (1913).
2. See, for example, C. B. Walker, Phys. Rev. 103, 547 (1956).
3. M. Elcombe, Bull. Am. Phys. Soc. 10, 435 (1965).

4. M. Elcombe, private communication, 1965. Miss Elcombe very kindly provided her calculations for 5 different values of the reduced wave vector. We have taken the liberty of drawing smooth curves through these points.

5. L. Van Hove, Phys. Rev. 89, 1189 (1953).

D. FERMI SURFACES OF GALLIUM SINGLE CRYSTALS BY THE SIZE EFFECT

The Fermi surface of Gallium single crystals has been investigated by using the size effect. This is due to the small thickness of the sample which is comparable with the radius of the electronic orbit. The result has been compared with the Fermi surface derived previously by the author from the ultrasonic attenuation at microwave frequencies.[1]

The experimental arrangement is shown in Fig. II-9. Metallic Gallium of 99.9999% purity was purchased from the United Chemical and Mineral Corporation, New York.

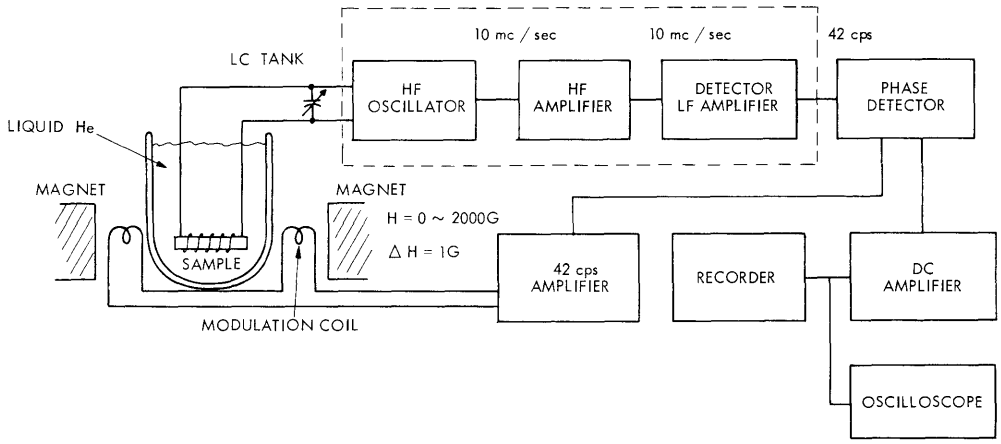

Fig. II-9. Experimental arrangement.

A Gallium crystal was grown between two lucite slabs, with a milar film used to fix the thickness of the crystal. Crystals of 0.15-1 mm thickness and 2 cm × 1 cm area have been made by this technique. The crystal axis has been checked by x-ray and the angles verified within one degree. Enamel wire No. 38 was wound directly on the sample to make a coil in an LC tank circuit in a high-frequency oscillator. The frequency of the oscillator was set to 5-10 Mc/sec which is small enough compared with the cyclotron frequency of the electron (1-3 Gc/100 gauss) and large enough, so that the skin depth of the high-frequency wave stays much less than the sample thickness.

The DC magnetic field was set parallel to the flat surfaces of the sample, and the electron then rotates in a plane perpendicular to the flat surfaces. The electronic orbit intersects both surfaces when the DC field, H, reaches

$$H_o = \frac{2\hbar c k}{de}, \qquad (1)$$

where d is the sample thickness.

If the field is swept through H_o, there is a singularity in the surface impedance of the Gallium slab at H_o, hence the Q of the coil shows a singularity of this point. The change in Q appears in the amplitude of the HF oscillator output. This output is high-frequency amplified and supplied to the recorder after detection and DC amplification. To improve the signal-to-noise ratio, the DC field was modulated at 42 cps. The signal output was then proportional to the derivative, dA/dH, of the absorption with respect to the field.

The skin depth at 42 cps is larger than the sample thickness so the modulation field penetrates through the sample. The wave vector of the electron located at the extremum point in the Fermi surface can be found from H_o through Eq. 1.[2] By rotating the slab in the plane parallel to the field, the extremal cross sections of the Fermi surface were found.

Figure II-10 shows the dA/dH vs H curve for a sample, 0.335 mm thick, $\theta = 15°$ and with a modulation field strength of 1 gauss where θ is the angle between the magnetic

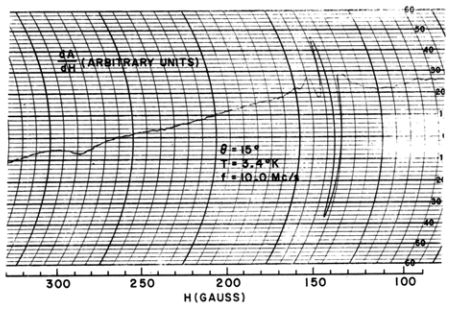

Fig. II-10. Detected signal vs magnetic field.

field direction and the b axis. A second harmonic is evident in Fig. II-10 at $H \approx 310$ gauss. Third and higher harmonics could not be identified because of the poor signal-to-noise ratio.

The wave vectors of this sample are plotted in Figs. II-11. This is the Fermi surface in the ky-kz plane, if the center of the extremum orbit coincides with the center of the Brillouin zone.

In the previous report, to find the Fermi surface by ultrasonic attenuation we used Tepley's[3] value for sound velocity, $v_a = 3.73 \times 10^5$ cm/sec which he found using an oscilloscope and sound pulses.

If we use instead $v_a = 4.62 \times 10^5$ cm/sec, which corresponds to the sound velocity along the c axis found by Tepley, then the Fermi surface found in the ultrasonic experiment becomes very close to that obtained in the present experiment. This fact suggests

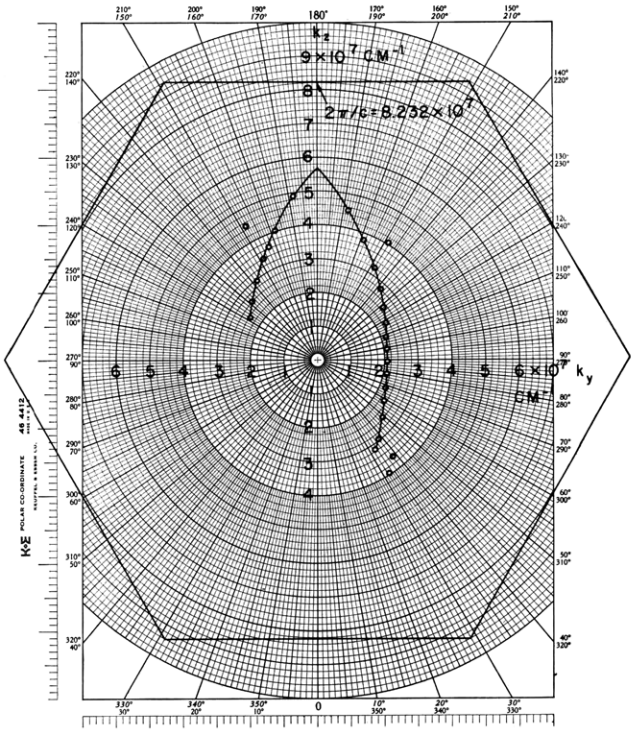

Fig. II-11. Fermi surface derived from sample No. 7/8-1.

that the size effect may provide a good method for measuring the sound velocity in metals together with the ultrasonic attenuation.

A. Fukumoto

References

1. A. Fukumoto, Quarterly Progress Report No. 78, Research Laboratory of Electronics, M.I.T., July 15, 1965, pp. 15-19.
2. T. F. Gantmakher, Soviet Phys. – JETP 17, 549 (1963).
3. N. Tepley, Ph.D. Thesis, Department of Physics, M.I.T., 1963.